NASA-CR-176262
19860000843

TMS paper selection

PAPER NO.

F84-15

N86-10310

A SIMPLE METHOD OF OBTAINING CONCENTRATION DEPTH-PROFILES FROM X-RAY DIFFRACTION

by

K. E. WIEDEMANN

J. UNNAM

THE METALLURGICAL SOCIETY OF AIME
420 Commonwealth Drive, Warrendale, PA 15086 • 412/776-9000

A SIMPLE METHOD OF OBTAINING CONCENTRATION DEPTH-PROFILES FROM X-RAY DIFFRACTION

K. E. Wiedemann and J. Unnam

Analytical Services & Materials, Inc.
103 Winder Road
Tabb, Virginia 23602
USA

Abstract

Although the construction of composition profiles from x-ray intensity bands is an important and reliable technique, it has not been routinely practical because it required hours of computer time and complicated optimization routines. The Intensity-Band-to-Composition-Profile-Transformation proposed here utilizes a solution that can be evaluated even with a hand-held calculator. This technique is applicable to thin films and thick specimens for which the variation of lattice parameters, linear absorption coefficient and reflectivity with composition are known. A deconvolution scheme including corrections for the instrumental broadening and a Kα-doublet is discussed.

Introduction

The x-ray diffraction intensity band is a compositionally broadened diffraction peak. The ideal diffraction peak is sharp, narrow, and symmetric. Such a peak is observed by diffraction from a homogeneous phase in which the inter-atomic spacings are uniform. The intensity band is observed by diffraction from a nonhomogeneous phase in which the variations in composition result in a range of inter-atomic spacings.

The basic relationships between the x-ray diffraction band and the composition-depth profile have been understood for some time. An intriguing aspect of these relationships is the hyper-sensitivity of the intensity band to the shape of the profile. A number of techniques have been developed by investigators seeking to use this sensitivity to construct high precision profiles (1-3). The difficulties encountered have been twofold: complications due to intensity broadening, and prohibitive computational requirements. The seriousness of these difficulties has restricted the use of these techniques to academic pursuits.

The entire breadth of the intensity band is not due solely to compositional broadening. Instrumental broadening and specimen broadening also contribute to the intensity band. To interpret the intensity band correctly this non-compositional broadening must be accounted for. In the past simulation techniques have most successfully handled this problem. The compositional broadening is calculated from an assumed composition-depth profile and convoluted with an analytic broadening function. The assumed composition-depth profile is then varied by trial and error until there is adequate agreement between the simulation and the experimental intensities (2).

The simulation techniques have also been the most accurate interpreters of the intensity band. However, the complexity of the calculations and its trial and error dependence necessitated lengthy calculations that even with high-speed computers and non-linear regression have been prohibitively long (3).

The technique presented here has simple computational requirements and is as accurate and flexible as the simulation techniques. It first removes the specimen and instrumental broadening by deconvolution and then transforms the deconvoluted intensities into a composition-depth profile using the relationships developed in the theory section of this paper.

Theory

Deconvolution

In a diffractometer the diffracted x-ray intensity is measured as the number of x-ray quanta per second incident on the detector, or, when nearly monochromatic x-rays are being used, it is more conveniently expressed as power. This power has been broadened by various sources from the instrument and sample. We are interested in isolating the compositional broadening from all other sources.

The deconvolution technique is predicated on expressing the broadened power as a summation. To do so we must first adopt two artificial concepts. The first is that the broadened power, which has been collected at arbitrary 2θ positions, represents the power-per-degree 2θ as if it had been collected with an infinitely narrow receiver slit. The second concept

is that the unbroadened power has the form of an array of contiguous channels of arbitrary widths and that the power-per-degree within each channel is constant.

Using these concepts we can consider the following convolution equation:

$$\left(\frac{dP_b}{d2\theta}\right)_n = \left[\int_{-\infty}^{+\infty} g(2\theta_n - t)\,\frac{dP}{d2\theta}\,dt\right] + \varepsilon_n \qquad n = 1,\ldots,N \tag{1}$$

where $\frac{dP_b}{d2\theta}$ is the broadened power-per-degree 2θ, g is a normalized distribution function, $\frac{dP}{d2\theta}$ is the unbroadened power-per-degree 2θ, and ε is an error term that is associated primarily with counting statistics. Because the form of the unbroadened power is an array of contiguous channels, the broadened power may also be expressed by:

$$\left(\frac{dP_b}{d2\theta}\right)_n = \left[\sum_{m=1}^{M} G_{nm}\left(\frac{dP}{d2\theta}\right)_m\right] + \varepsilon_n \tag{2}$$

where $\frac{dP}{d2\theta}_m$ is the power-per-degree 2θ for channel m and G_{nm} is a dimensionless quantity given by:

$$G_{nm} = \begin{cases} m = 1 & \displaystyle\int_{-\infty}^{b_1} g(2\theta_n - t)dt \\ m \neq 1,\ m \neq M & \displaystyle\int_{b_{m-1}}^{b_m} g(2\theta_n - t)dt \\ m = M & \displaystyle\int_{b_{M-1}}^{+\infty} g(2\theta_n - t)dt \end{cases} \tag{3}$$

where the limits of integration, b_m, are the channel boundaries.

It can be shown from Eq. (2) that for the Lagrange function

$$F = \sum_{n=1}^{N} \varepsilon_n^2 + \sum_{s=1}^{S} \mu_s \phi_s \tag{4}$$

where μ_s is a Lagrange multiplier and ϕ_s is an arbitrary constraint, reasonable values for $\left(\frac{dP}{d2\theta}\right)_m$ are given by:

$$\left(\frac{dP}{d2\theta}\right)_m = \left(\frac{dP}{d2\theta}\right)^*_m + \sum_{\ell=1}^{M} [F'']^{-1}_{\ell m} F'_\ell \qquad (5)$$

where $\left(\frac{dP}{d2\theta}\right)^*_m$ is a suitable estimate of the unbroadened power, F'_ℓ are the first partials of the Lagrange function with respect to the unbroadened power-per-degree 2θ, and $[F'']^{-1}_{\ell m}$ is the matrix inverse of the array of second partials of the Lagrange function with respect to unbroadened power-per-degree 2θ.

When applied in an iterative fashion Eq. (5) will eventually yield reasonable values for the unbroadened power provided that the Lagrange multipliers, μ_s, and the arbitrary constraints, ϕ_s, are properly chosen.

It is necessary that at least one constraint be employed to keep the sum of errors squared, $\sum_{n=1}^{N} \varepsilon_n^2$, from vanishing. If this happens the unbroadened power-per-degree 2θ becomes dominated by large spurious oscillations. We suggest that an appropriate constraint would be:

$$\phi_1 = \left\{ \sum_{\ell=1}^{M} \left[\left(\frac{dP}{d2\theta}\right)^*_\ell - \left(\frac{dP}{d2\theta}\right)_\ell \right]^2 \right\} - R^2 = 0 \qquad (6)$$

where R^2 is the square of the n-fold distance between the successive iterations of Eq. (5). This constraint causes the convergence of Eq. (5) to progress uniformly. Suitable Lagrange multipliers for this constraint lie between 0.1 and 1.

If the normalized distribution g is the non-compositional broadening measured at the intensity-band extremes or from homogeneous phases, then the unbroadened power given by Eq. (5) has only compositional broadening remaining. The normalized distribution g is not restricted to any particular analytic form and, hence, can be chosen to fit any line-shape, singlet or doublet.

Intensity Band to Composition-Depth Profile Transformation

The technique employed here is based on the well-known equation for the power diffracted by an infinitesimally thin volume element at a depth x:

$$dP = 2P_o \delta \lambda^{-1} \exp(\eta_x) Q \, dx \qquad (7)$$

where dP is the diffracted power (energy per unit time), P_o is the incident beam power, δ is the d-spacing, Q is a pseudo-reflectivity term, λ is the x-ray wavelength, η_x is an absorption term, and dx is the thickness of the volume element.

The pseudo-reflectivity term, Q, for a polycrystalline material and a monochromator with a Bragg angle of 2α is given by:

$$Q = \frac{r_e^2 \lambda^3}{V^2} \frac{1 + \cos^2 2\alpha \cos^2 2\theta}{\sin 2\theta (1 + \cos^2 2\alpha)} F^2 p \exp(-2M) \tag{8}$$

where $r_e^2 = 7.94 \times 10^{-26}$ cm^2, V is the volume of the unit cell, F is the structure factor, p is the multiplicity, and the exponential term is the Debye-Waller thermal factor.

The absorption term is given by:

$$\eta_x = -4\delta\lambda^{-1}\left(\int_0^x \mu \, dx + \mu^* t^*\right) \tag{9}$$

where μ is the linear absorption coefficient and t^* is the thickness of the overlayer, if present, and μ^* is the linear absorption coefficient for the overlayer. The first derivative of η_x with respect to δ is given by:

$$\frac{d\eta_x}{d\delta} = -4\mu\delta\lambda^{-1} (1 + \gamma_x)\left(\frac{dx}{d\delta}\right) \tag{10}$$

where the d-spacing gradient term γ_x is given by:

$$\gamma_x = (\mu\delta)^{-1}\left(\int_0^x \mu \, dx + \mu^* t^*\right)\left(\frac{d\delta}{dx}\right) \tag{11}$$

Multiplying by the integration factor $[2\mu Q^{-1}(1 + \gamma_x)]$, Eq. (7) becomes:

$$\frac{dP}{d\delta} \frac{2\mu}{Q} (1 + \gamma_x) \, d\delta = -P_o \exp(\eta_x) \, d\eta \tag{12}$$

We shall define a modified diffracted power $\mathbb{P}_x$ as the integration of either side of Eq. (12) over the range between δ_o, the d-spacing of the surface and δ_x, the d-spacing of the material at the depth x. Thus:

$$\mathbb{P}_x = \int_{\delta_o}^{\delta_x} \left(\frac{dP}{d\delta}\right) 2\mu Q^{-1}(1 + \gamma_x) \, d\delta \tag{13}$$

and

$$\mathbb{P}_x = P_o \left[\exp(\eta_o) - \exp(\eta_x)\right] \tag{14}$$

where

$$\eta_o = -4\delta_o \lambda^{-1} \mu^* t^* \tag{15}$$

The quantity $\left(\frac{dP}{d\delta}\right)$ is equal to the counts (x-ray quanta) per second measured by the detector. All of the quantities in Eqs. (13) and (14) are explicitly known except for x and γ_x. γ_x, however, is very small when $t^* = 0$ and can be approximated by zero to a very high precision. Thus, solving for x in Eq. (14):

$$x = \int_{\delta_o}^{\delta_x} \mu^{-1} \frac{d}{d\delta} \left[-\lambda(4\delta)^{-1} \ln(1 - \exp(-\eta_o) P_o^{-1} \mathbb{P}_x)\right] d\delta \tag{16}$$

Usually it is not convenient to determine P_o experimentally. A numerical approximation consistent with Eq. (14) can be obtained from

$$P_o = \mathbb{P}_\infty \exp(-\eta_o) \tag{17}$$

because $\exp(\eta_\infty) = 0$. $\mathbb{P}_\infty$ is the integration of Eq. (13) over the entire intensity band--i.e., it is the total modified power.

For thin film P_o must be calculated in an iterative fashion from the expression:

$$P_o = \mathbb{P}_t \left[\exp(\eta_o) - \exp(\eta_t)\right]^{-1} \tag{18}$$

where $\mathbb{P}_t$ is the total modified power analogous to $\mathbb{P}_\infty$

$$\eta_t = -4\delta_t \lambda^{-1} \left(\langle\mu\rangle t + \mu^* t^*\right) \tag{19}$$

t is the film thickness, $\langle\mu\rangle$ is the average linear absorption coefficient, and δ_t is the d-spacing corresponding to the backside of the film. Initially a value is assumed for $\langle\mu\rangle$, P_o is calculated from Eq. (18), and the profile evaluated using Eq. (16). Subsequently $\langle\mu\rangle$ is calculated by:

$$\langle\mu\rangle = \frac{1}{t} \int_o^t \mu \, dx \tag{20}$$

and P_o and the profile are reevaluated. The average linear absorption coefficient, P_o, and the profile are evaluated iteratively until the change in the profile between successive iterations is satisfactorily small (5).

Discussion

Consider a flat sample containing a nonhomogeneous phase such as the one depicted in Figure 1. In this example the nonhomgeneous phase is the substrate and a second phase is an overlayer. The composition gradient is normal to the free-surface and the substrate is, for x-ray purposes, infinitely thick.

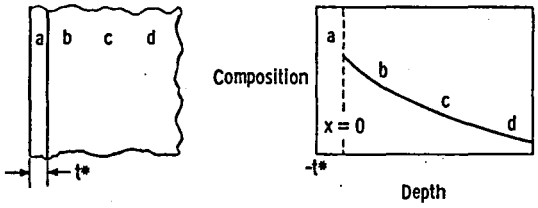

a. Overlayer
b. Near surface } Substrate - single phase with
c. Shallow interior } a composition gradient
d. Deep interior

Figure 1. A specimen with a composition gradient in the substrate. The overlayer and substrate are different phases.

When the incident beam enters the sample, as depicted in Figure 2, no diffraction pertinent to the intensity band occurs in the overlayer. The sole effect of the overlayer is absorption. Diffraction occurs in the substrate. X-rays diffracted near the surface undergo very little absorption and therefore the diffracted intensity from the near surface is strong. Diffraction from the interior is weaker because both the incident beam and the diffracted beams are heavily absorbed - diffraction from the deep interior is completely lost. The angle of diffraction is determined by the composition. Each point along the composition gradient will diffract the x-rays at a slightly different angle; the combined effect is the intensity band.

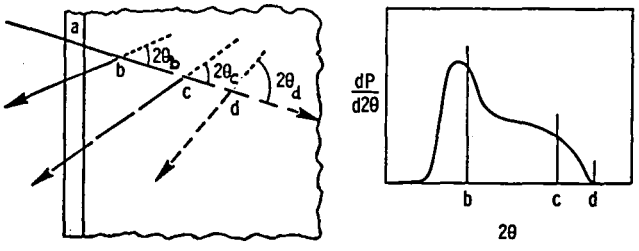

a. Overlayer : no diffraction
b. Near surface : strong diffraction
c. Shallow interior: weak diffraction
d. Deep interior : completely absorbed diffraction

Figure 2. Diffraction from a specimen with a composition gradient. Change of 2θ with depth is continuous.

If we assume that the composition gradient is normal to the specimen surface and that the composition profile is monotonic then the transformation outlined in the theory section of this paper will construct the composition-depth profile from the intensity band. If the phase being examined is in the form of a thin film it must be uniformly thick. The accuracy of the transformation will then depend on how well the thickness is known. A phase is considered to be in the form of a thin film for x-ray purposes if there is perceptible diffracted intensity from all parts of the phase.

Because this is not an elemental technique the results will be ambiguous except for binary composition depth profiles. Quasi-binary scenarios such as the dissociation and absorption of a gas by a metal alloy are also unambiguous, but cases where there are several diffusing species can only be analyzed under special circumstances which are beyond the scope of this paper.

Currently this technique is being employed in diffusion, kinetic modeling, and phase transformation studies. Its potential use is much broader including semiconductor and quality control applications because of its high resolution and its ability to discriminate phases.

The working depth can be varied by changing the wavelength of the incident beam. For most materials the working depth can be varied from a few hundred angstroms to several millimeters. This is determined by the linear absorption coefficient and is approximately equal to $(2\mu)^{-1}$.

Duplicate specimens of oxidized titanium were analyzed and the results of the analysis were compared. Figure 3 presents the composition-depth profiles of three sets of duplicate specimens. Specimens in a duplicate set were prepared independently. Differences between composition-depth profiles for duplicate specimens reflect experimental error as well as the inherent precision of the technique.

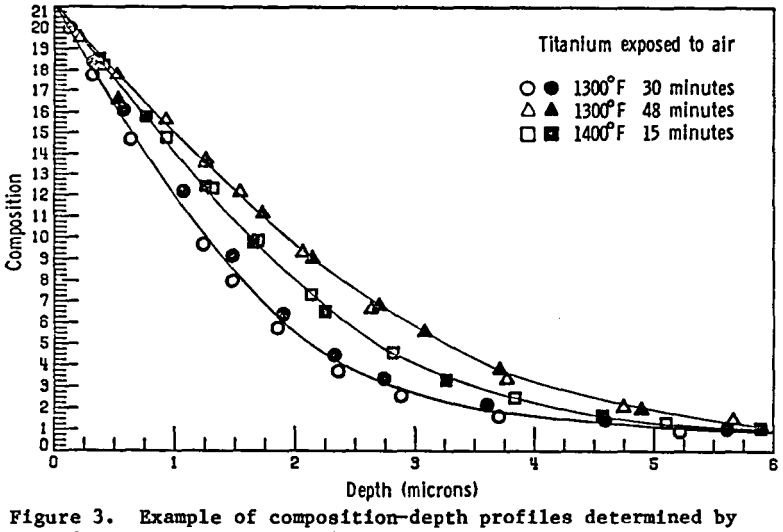

Figure 3. Example of composition-depth profiles determined by transformation. Use of replicates is, for the first time, practical because of the ease of data acquisition and analysis.

In order to describe the effect of counting statistics on the composition depth profile consider again the expression for the modified diffracted power, Eq. (13). Because the standard deviation of L counts is $\sqrt{L}$ counts (assuming a Poisson distribution),

$$\mathbb{P}_x^{\pm} = \int_{\delta_o}^{\delta_x} \frac{d}{d\delta} (L \pm 1.65\sqrt{L})/\tau \;\; 2\mu Q^{-1}(1 + \gamma_x)\, d\delta \tag{21}$$

where $\mathbb{P}_x^{\pm}$ are the 90% confidence limits for $\mathbb{P}_x$, L is the number of counts, and γ is the counting time. The 90% confidence limits on the depth are given by:

$$x^{\pm} = \int_{\delta_o}^{\delta_x} \mu^{-1} \frac{d}{d\delta} \left\{ -\lambda(4\delta)^{-1} \ln \left[1 - \exp(-\eta_o)\, P_o^{-1}\, \mathbb{P}_x^{\pm} \right] \right\} d\delta \tag{22}$$

where $x^{\pm}$ are the 90% confidence limits on the depth. An example calculation of $x^{\pm}$ is presented in Figure 4. Errors in the profile due to counting statistics tend to be small, being the smallest at $x = 0$ and increasing with depth.

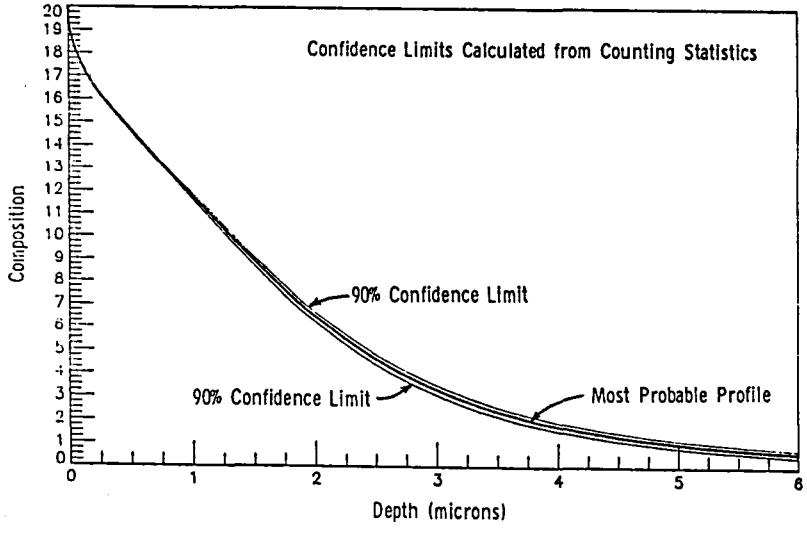

Figure 4. Confidence limits calculation for an intensity band transformation. It is possible to achieve good precision in the composition-depth profile using continuous scan data--opposed to point counting--as demonstrated by the transformation of an intensity band collected at a scan speed of 0.1° per minute over 1.5°.

The diffractometer used should have moderate to high resolution. Diffracted beam monochromators that can separate the $K\alpha_1$ component are desirable. It is also good to choose the narrowest receiver slit available and in general to do all things that aid resolution.

The use of high angle peaks and high resolution diffractometers will help preserve the detail contained in the intensity band. The more non-compositional broadening present, the more one will need to rely upon the deconvolution routine to construct meaningful profiles. Failure to deconvolute adequately will produce errors at the extreme compositions as well as masking the detailed structure of the composition-depth profile. Figure 5 is a composite plot of the transformation of an intensity band before and after deconvolution. The transformation of the intensity band before deconvolution has errors at the extreme compositions.

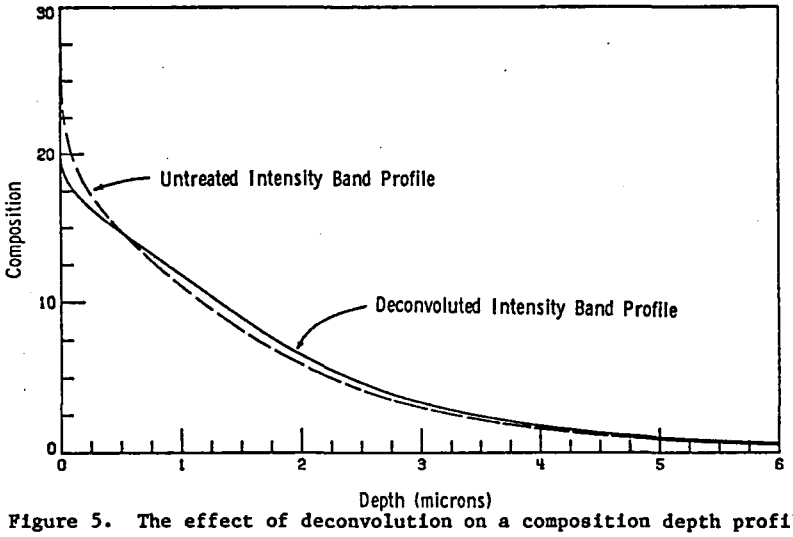

Figure 5. The effect of deconvolution on a composition depth profile.

By making a series of approximations and simplifications, including Q = constant and μ = constant, it is possible to write:

$$x_n = \frac{-\sin\theta_n}{2\mu} \ell n \left[1 - \sum_{i=1}^{n} \left(\frac{dP}{d\delta}\right)_i \Delta\delta_i \Big/ \sum_{j=1}^{N} \left(\frac{dP}{d\delta}\right)_j \Delta\delta_j \right] \qquad (23)$$

where x_n is the depth, $\left(\frac{dP}{d\delta}\right)_i$ is the counts per second at the detector arranged in the order such that $\left(\frac{dP}{d\delta}\right)_1$ corresponds to δ_o, and $\left(\frac{dP}{d\delta}\right)_N$ corresponds to δ_∞. This expression is similar in several points to that of Pines (6).

This expression is sufficiently simple so that it could be evaluated for small data sets with a hand-held calculator. Assuming that non-compositional broadening is negligible we may skip the deconvolution step. An example calculation using Eq. (23) is given in Table I and the results

are plotted in Figure 6 against the more complete treatment using deconvolution and Eq. (16). The agreement is excellent except for a small depth (less than 0.3 μm) where the neglecting of instrumental broadening has a significant effect.

Table I. An Example Calculation of Composition Depths Profile Using Eq. (23).

$2\theta_i$	$\left(\frac{dP}{d\delta}\right)_i$	δ_i	$\Delta\delta_i$	$\sum_{i=1}^{n}\left(\frac{dP}{d\delta}\right)_i \Delta\delta_i$	x_n(μm)	Comp. at %
37.47	0.66	2.3983	-0.0022	-0.0014	0.006	25.93
37.54	1.06	2.3939	-.0040	-.0057	.026	23.81
37.60	2.03	2.3903	-.0037	-.0131	.061	21.89
37.66	3.88	2.3866	-.0040	-.0285	.135	19.90
37.73	6.81	2.3823	-.0037	-.0534	.262	17.52
37.78	9.28	2.3793	-.0030	-.0816	.417	15.81
37.83	10.01	2.3763	-.0039	-.1209	.661	14.12
37.91	10.13	2.3714	-.0042	-.1636	.972	11.47
37.97	9.51	2.3678	-.0048	-.2093	1.377	9.56
38.07	8.50	2.3618	-.0066	-.2651	2.046	6.63
38.19	7.55	2.3547	-.0062	-.3122	2.912	3.65
38.28	6.93	2.3494	-.0047	-.3450	3.922	1.92
38.35	6.19	2.3452	-.0038	-.3687	5.331	.93
38.41	4.91	2.3417	-.0029	-.3829	7.574	.36
38.44	2.06	2.3394	-.0023	-.3876	10.482	.13
38.48	.34	2.3372	-.0025	-.3884	12.888	.04
38.53	.22	2.3344	-.0014	-.3887	∞	-

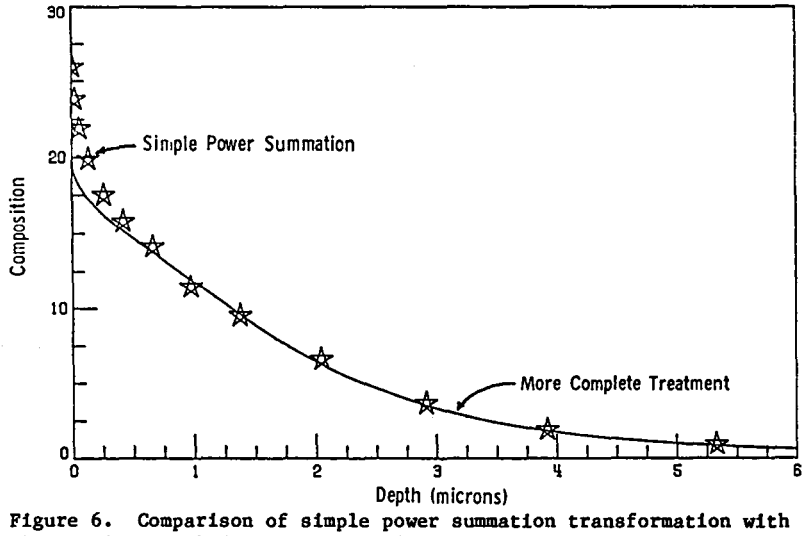

Figure 6. Comparison of simple power summation transformation with the complete technique. The simple power summation transformation is useful for checking and quick analysis. The agreement is largely fortuitous because the various errors tend to cancel in this example.

Concluding Remarks

Obtaining the composition profiles from x-ray diffraction intensity bands is easy, both experimentally and analytically. Though the technique is not elemental and hence is usually restricted to binary or quasi-binary profiles, the inherent discrimination of phases enables observation of clear composition-depth profiles when overlayers or sublayers are present. And finally, the composition-depth profiles found by this technique are very precise in working depths that range from angstroms to millimeters.

Acknowledgement

The authors are grateful to the NASA Langley Research Center for the support of this research.

References

1. D. R. Tenney, J. A. Carpenter, and C. R. Houska, "X-Ray Diffraction Technique for the Investigation of Small Diffusion Zones," Journal of Applied Physics, 41 (11) (1970), pp. 4485-4491.

2. J. Unnam, J. A. Carpenter, and C. R. Houska, "X-Ray Diffraction Approach to Grain Boundary and Volume Diffusion," Journal of Applied Physics, 44 (5) (1973), pp. 1957-1967.

3. K. E. Wiedemann, "Diffusion of Oxygen and Nitrogen in Titanium and the Use of Ti_3Al as an Oxidation Inhibitor," Thesis, Virginia Polytechnic Institute and State University, 1983.

4. K. E. Wiedemann and J. Unnam, "TIBAC - Transformation of an Intensity Band for the Analysis of Composition," LAR-13356, COSMIC, University of Georgia, 1984.

5. B. Ia. Pines and E. F. Chaidouski, Doklady, Academie Nauk. SSSR, 111 (1956), pp. 1234-1237.

End of Document